Journal Pre-proofs

Solar sail propulsion limitations due to hydrogen blistering: Progression of reflectance decrease

Erik M. Klein, Patric Seefeldt, Maciej Sznajder, Oliver Hetherington

PII: S0273-1177(25)01488-7
DOI: https://doi.org/10.1016/j.asr.2025.12.061
Reference: JASR 19127

To appear in: *Advances in Space Research*

Received Date: 8 May 2025
Revised Date: 12 December 2025
Accepted Date: 16 December 2025

Please cite this article as: Klein, E.M., Seefeldt, P., Sznajder, M., Hetherington, O., Solar sail propulsion limitations due to hydrogen blistering: Progression of reflectance decrease, *Advances in Space Research* (2025), doi: https://doi.org/10.1016/j.asr.2025.12.061

Graphical Abstract

Solar sail propulsion limitations due to hydrogen blistering: Progression of reflectance decrease

Erik M. Klein, Patric Seefeldt, Maciej Sznajder, Oliver Hetherington

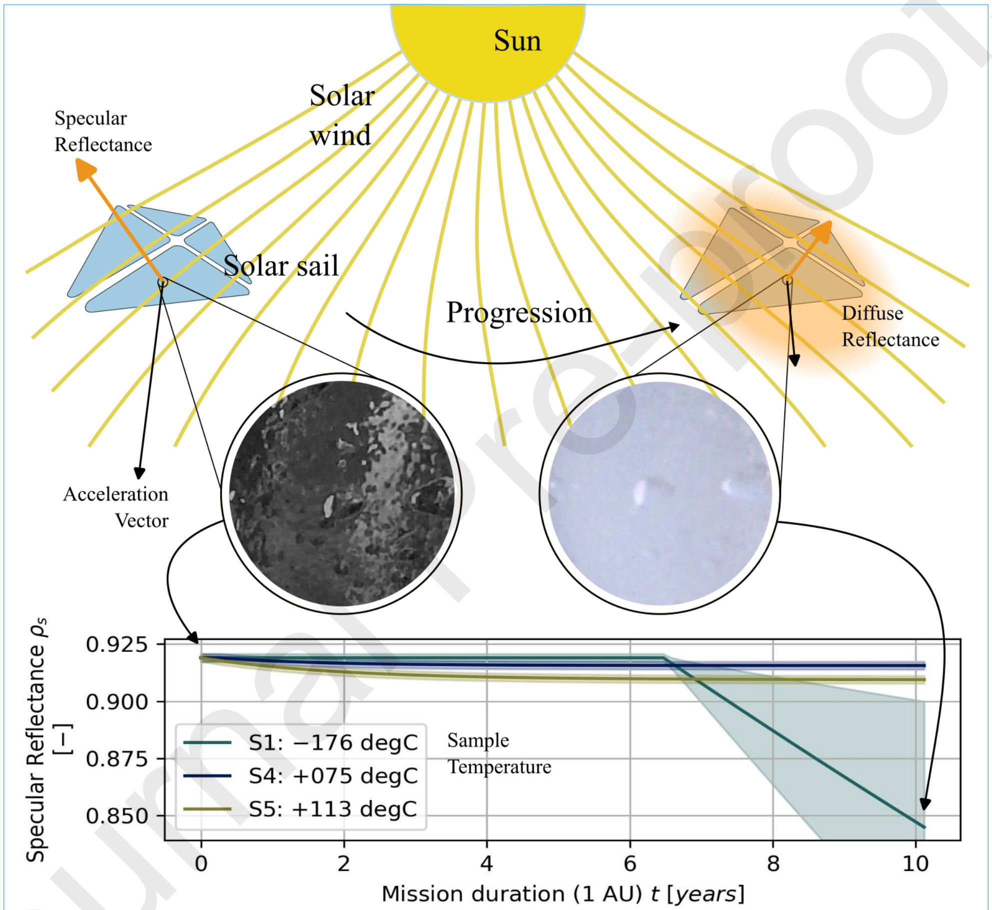

Solar sails, made from metallized thin films, are a developing technology for interplanetary transportation, but their membranes degrade when exposed to solar wind protons and other radiation. Previous research highlighted significant material deterioration under simulated space conditions in the time frame of one solar cycle. This study aims to better understand how specular reflectance changes over time due to proton irradiation and relate this to different mission scenarios in terms of total fluence for constant temperature. By analyzing time-lapse images of radiation tests and spectrometric measurements, the progression of reflectance over fluence and mission duration is determined, offering improved predictions of solar sail performance for future missions.

Highlights

Solar sail propulsion limitations due to hydrogen blistering: Progression of reflectance decrease

Erik M. Klein, Patric Seefeldt, Maciej Sznajder, Oliver Hetherington

- Progression of thermo-optical properties in dependence of fluence
- Possibility to predict via semi-empirical equations the evolution of the specular reflectance and hence the performance of solar sails
- Investigation on the temperature dependence of thermo-optical properties during proton irradiation
- Novel flux models predict reflectance degradation in space to be slower than expected

Solar sail propulsion limitations due to hydrogen blistering: Progression of reflectance decrease

Erik M. Klein[a,*], Patric Seefeldt[a], Maciej Sznajder[b,c], Oliver Hetherington[d,a]

[a] *German Aerospace Center (DLR), Institute of Space Systems, Mechanics and Thermal Systems, Robert-Hooke-Str. 7, Bremen, 28359, Bremen, Germany*
[b] *Janusz Gil Institute of Astronomy, University of Zielona Góra, Licealna 9, Zielona Góra, 65-417, Poland*
[c] *PW Sznajder, P3RUN - Radiation Hardness Assurance & Data Science Expertise, Dolina Zielona 19A, Zielona Góra, 65-154, Poland*
[d] *TU Delft, Postbus 5, Delft, 2600 AA, South Holland, Netherlands*

Abstract

Solar sails are an advancing technology for transportation in interplanetary space. Metallized thin films are commonly used to build their membranes. During their lifetime the functional surfaces are exposed to various types of radiation, among them the low energy solar wind (SW) protons and other element ions. In Sznajder et al. (2020), it was investigated what influence the recombination processes of SW protons with metal electrons has on the thermo-optical properties of the sail membrane. The results indicated a harsh degradation of membrane material samples when subjected to the laboratory simulated interplanetary space solar wind conditions, especially for exposure at low temperatures. However, more recent studies Sznajder (2023) indicate that the blistering process in this severity would take several years to appear in space.

In view of the drastic degradation observed due to proton irradiation, it is the aim of this work to understand the development of the specular reflectance over the accumulated fluence. Furthermore, this data is mapped to certain mission scenarios, so that an understanding of the process with its change of specular reflectance over mission time is gained.

Specimens reflectance and temperature over fluence data was further evaluated to gain knowledge on the processes during irradiation. Therefore,

*Corresponding author: erik.klein@dlr.de

time-lapse pictures of the radiation tests were analysed. In particular, the brightness of pixels and its change from picture to picture were evaluated. This data was combined with spectrometric measurements taken before and after the test such that a progression over time or fluence, respectively, could be derived.

Improved evaluation of previously presented experiments are given. The progression of the specular reflectance over fluence and hence a mission time is derived. The analyses allows a more accurate assessment of the performance of solar sails in dependence of the mission scenario (e.g. fluence and temperature) for future missions.

Keywords: Solar sailing, Hydrogen blistering

1. Introduction

Solar sailing relies on the specular reflection efficiency of its membrane material to change orbit energy. Thin aluminized polymer films are commonly considered as lightweight membrane reflector material. However, due to the presence of low energetic protons in the solar wind, these reflectors lose their specular reflectance due to hydrogen blistering. This phenomenon occurs when protons combine with free electrons of the metal lattice, forming microscopic bubbles, filled with hydrogen molecular gas, on the surface, thus changing the surface from specular to diffuse reflectivity. The aim of the presented work is to quantify the reflectance loss over mission time to understand its impact on solar sail missions better.

Results presented here are a continuation of a series of scientific effort in understanding of the so-called hydrogen blistering phenomenon. This process refers to formation of tiny pockets filled with molecular hydrogen gas just below exposed metallic surface. Hydrogen forms from recombination processes (Hagstrum, 1954; Sols and Flores, 1984; Eichler, 2005) of solar wind protons and electrons present in a target material. Hence, in order to form hydrogen, energy of incident protons must be low enough to stop within target material. If the energy is too high, protons pass though the material to the underlying substrates or they pass though the whole membrane.

Previous work took into consideration proton fluence (Sznajder et al., 2015), a magnitude of proton flux (Sznajder et al., 2018), and a target material temperature (Sznajder et al., 2020) on the phenomenon. The here presented work continues this effort towards more precise prediction of the thermo-optical properties of functional surfaces, in specific aluminized solar sail membranes. This will enhance the solar sail mission designer to consider the degradation of the solar sail membrane into the trajectory of the exploration mission.

1.1. Hydrogen Blistering

Hydrogen blistering is a phenomenon classified under hydrogen embrittlement (HE) (Myers et al., 1992), causing irreversible changes in material properties due to hydrogen agglomeration within the metal lattice. In space, hydrogen is formed in metals through recombination processes of solar wind protons and electrons within the metal lattice. Solar sail membrane materials are continuously exposed to proton flux, leading to increasing concentrations of recombined hydrogen within their metallic layers. Blistering occurs as hydrogen agglomerates into H_2-clusters, appearing as small metallic pockets on the membrane surface, affecting its reflectivity. Radii of these blisters are in the μm-range (Sznajder et al., 2015). The process from forming hydrogen to H_2 until the blister cracks is shown in figure 1.

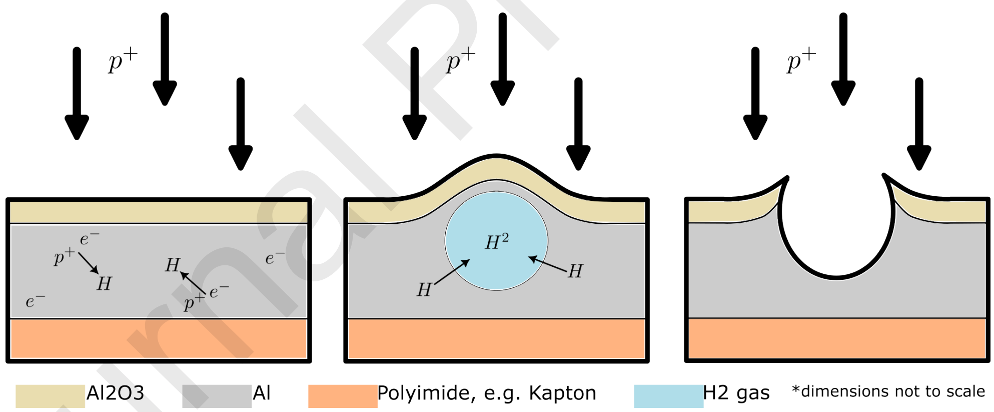

Figure 1: The figure shows the three steps to blistering and eventually cracking of the surface of the aluminized membrane. From left to right, initially the incident protons find free electrons inside the Al metal lattice and from hydrogen atoms. These atoms form together H_2 molecules and agglomerate in bubbles which, with further incident proton flux, grow until they crack the surface open, seen in the image on the right.

The membrane consists of a substrate, e.g. polyimide like Kapton, coated with some aluminized layer. The aluminized layer forms a oxide layer on top of the substrate still during production in atmosphere. The back side of the membrane, that is not used for acceleration, can be coated with other materials, e.g. chromium for higher emissivity, but aluminium is also possible.

Blistering occurs under specific environmental conditions including proton energy, flux, fluence magnitude, and specimen temperature. Proton energy must be low enough for protons to become trapped within the aluminium layer, with certain percentages being back-scattered or transmitted. Proton flux must be below a certain threshold to prevent cracking of the aluminium oxide layer acting as a diffusion barrier for recombined hydrogen. Proton fluence exceeding a certain threshold leads to blister formation on the aluminium surface. Temperature significantly influences blistering, with lower temperatures slowing down the process and higher temperatures accelerating it (Sznajder et al., 2020). Studies indicate that impurities, defects within the metal structure (Daniels, 1971), and crystallographic orientation (Milacek et al., 1968) can influence blister formation.

In the following, the underlying data, partly seen in Sznajder et al. (2020), will be shown and explained in section 2.1. Afterwards, the newly developed model to connect brightness and thermo-optical properties will be discussed in section 2.3 and lastly, results will be shown in section 3 and discussed in 4.

2. Methodology

The following sections will first give an overview over the conducted experiments, afterwards the irradiated fluence will be set in context creating a mission scenario and eventually the semi-empirical reflectance model will be explained.

2.1. Test

Previously, in Sznajder et al. (2020), solar sail foils were irradiated and evaluated for their thermo-optical changes in dependence of various temperatures. Summarizing information on the main key points of these experiments can be found in table 1. Irradiation was conducted inside the Complex Irradiation Facility (CIF) of the Institute of Space Systems (IRS) at the German Aerospace Center (DLR) Bremen (Renger et al., 2014).

Membranes under investigation have been glued onto a copper plate in order to enhance the thermal conduction and therefore improve temperature control. Unfortunately, trapped air, which was not visible unter atmosphere, formed bubbles in vacuum between membrane and copper plate. These can

Table 1: Thermo-optical properties of samples irradiated with 2.5 keV protons with a fluence of $2.2 \cdot 10^{17}$ $p^{+}cm^{-2}$ (Flux given as $2 \cdot 10^{12}$ $p^{+}cm^{-2}s^{-1}$). For the three shaded samples time-lapse photographs were available. The associated graphs are shown in figure 3. An uncertainty of 0.1% for the reflectance measurements needs to be considered. Additionally the characteristic acceleration (Char. Accel.) is given as provided by Sznajder et al. (2020). Each row in this table is one irradiation with identical proton source parameters, e.g. flux. The varied parameter has been the temperature of the sample indicated as radiation temperature (Rad. Temp.).

Sample	**Rad. Temp.** T [°C]	**Total Refl.** ρ [-]	**Specular Refl.** ρ_S [-]	**Char. Accel.** $a_c/a_{c_{ref}}$ [-]
Pristine	-	0.923	0.919	1
S1	-176.0	0.693	0.599	97.18
S2	-100.0	0.875	0.479	96.53
S3	31.6	0.895	0.781	99.67
S4	75.0	0.916	0.909	99.00
S5	113.0	0.917	0.904	99.97

be seen in figure 2. They have no influence on the conducted measurements because optical data has been averaged over an area significantly bigger than that of a bubble.

For cooling Liquid Nitrogen (LN_2) was used, heating was conducted using halogen lamps that heated the sample station from behind and by that the sample holder and the specimen. A controller keeps the sample temperature on the specified value by controlling the halogen lamps. Apart from temperature all process parameter have been kept identical between irradiations, hence reproducinility is given.

The time-lapse photographs created during these experiments were used to extract the brightness data. Exemplary images of sample S1 before and after can be seen in figure 2. In order to get a uniform value for the brightness independent of wavelength, images were transformed into grey arrays. Unirradiated area was digitally masked and the average value of the remainders was calculated. The pixel values were averaged due to the inhomogeneous illumination, which can be seen in figure 2B. For the sake of noise reduction, samples were digitally tracked and linear movement of the sample station or camera was corrected. Due to thermal expansion, it was possible, that the samples station rotated slightly during heating or cooling of samples. The effect of this, was minimised by maximizing the averaging area, such that reflections due to rotation stay inside the area of interest and thus do not change the average value. During irradiation temperature was constant, thus no rotation of the sample station, and hence the sample surface, occurred in this time.

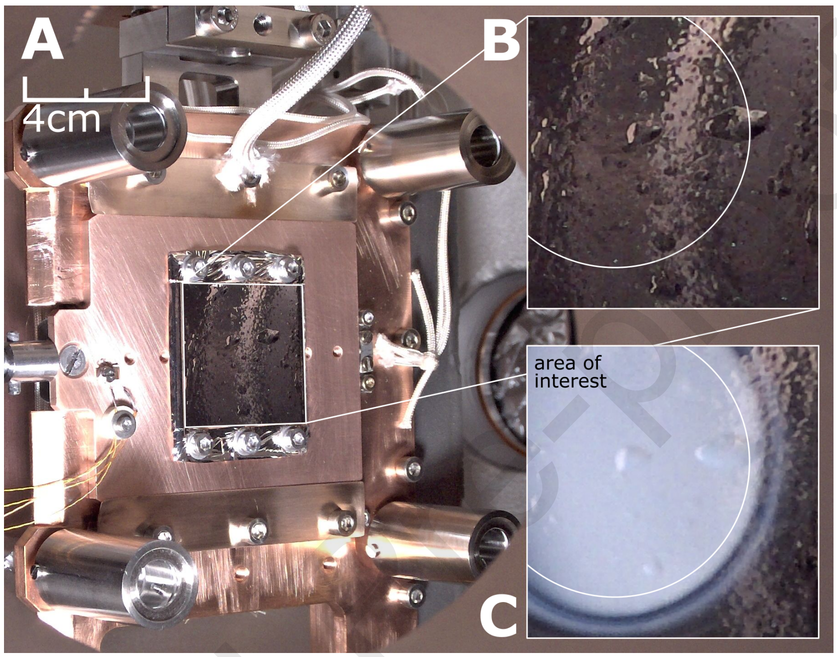

Figure 2: A) Sample S1 prior to radiation inside of the sample station of the CIF. Camera used was a DSLR Canon EOS 800D. B) and C) both being transformed into top view perspective, before and after irradiation, respectively. For brightness evaluation, only the pixels inside the area of interest, as marked above, were used. The setup will be more described in section 2.3. The side length of the detail images B) and C) is 4 cm each.

The resulting brightness data, before, during and after irradiation, can be seen in figure 3. Additionally the sample temperature is plotted. Unfortunately the initial cooling process of sample S1 has not been tracked. For samples S4 and S5, it can be seen, that the brightness decreased slightly during heating, e.g. in the beginning of each plot.

Further noteworthy are a few deviations of the temperature-brightness correlation in figure 3. Especially for sample S1, there are a few aberrations over the course of time. For sample S1 cooling dropped out shortly before irradiation finished. This manifests by increased brightening. After irradiation ended, this process stagnated to rates even lower than shortly before cooling failed. Later on, brightness reaches an maximum close to 40 hours after radiation start. At 50 hours after irradiation start, sample S1 has been heated briefly to 75 °C.

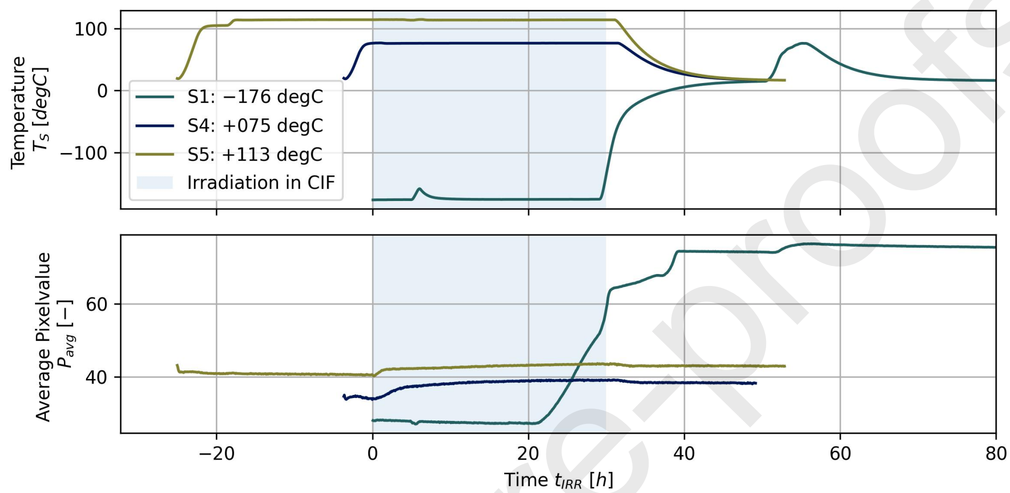

Figure 3: Initial data: Temperature and brightness plots for the investigated samples. $t_{IRR} = 0$ marks the beginning of irradiation. Duration of the irradiation is depicted by the light blue area. Sample S1 was annealed after irradiation at 75 °C which also had influence on the sample brightness.

2.2. Reference Mission Scenario

Since Sznajder et al. (2020), there were updated information made available. Previously, particle flux information in the low-energetic regime, concerning the solar wind, were sparse and with high uncertainty (Agency, 1993; Klein et al., 2022). It was shown, that the low-energetic proton flux was overestimated (Sznajder, 2023). In this subsection the connection between fluence and mission duration will be adapted to the new particles densities.

As in Sznajder et al. (2020) presented, low energetic particles are of interest. The lower the energy, the higher the likelihood they implant into the aluminized top layer. Using the spectra for solar cycle 23 from Klein et al. (2022), the mission flux can be calculated via

$$f_{Al} = \int_0^\infty f_d(E) \cdot P_{Al}(E)\, dE, \tag{1}$$

where f_d denotes the differential flux given in $p^+cm^{-2}s^{-1}keV^{-1}$ and P_{Al} the likelihood, that the protons gets stuck in the aluminium layer. P_{Al} was calculated using Stopping and Range of Ions in Matter (Ziegler et al., 2010) (SRIM). For various energies up to 15 keV SRIM simulations were conducted using the layer dimension of the Upilex membrane. The ratio of implanting (in the aluminium layer) protons to the total number of simulated protons gives than P_{Al}. The result can be seen in figure A.10.

Thus equation 1 returns $7.85{\cdot}10^8\ p^+cm^{-2}s^{-1}$ as average, $1.49{\cdot}10^9\ p^+cm^{-2}s^{-1}$ as maximum and $4.05 \cdot 10^8\ p^+cm^{-2}s^{-1}$ as minimum yearly average flux during solar cycle 23 with confidence interval of 50%. Thus a fluence of $2.2 \cdot 10^{17}p^+cm^{-2}$, as used here, equals 8.88 years, e.g. approx. 3/4th of one solar cycle, at one Astronomical Unit (AU). The Acceleration Factor (AF) was 2548 for the average scenario. The AF describes how much faster the laboratory test has been, compared to the environment. Depending on the specific mission trajectory, this can de- and increase. Further, here it is assumed, that all protons are incident orthogonally onto the surface. Tilting the particle beam decreases the projected penetration depth, such that more particle get stuck closer to the surface hence become relevant for hydrogen blistering. In the context of solar sailing, this is especially important, as these are usually always tilted for maneuvering (Dachwald et al., 2005; Dachwald, 2010), assuming the solar wind is incident in outward radial direction from the sun. For hemispherical flux characteristics this is important for the same reason.

2.3. Reflectance Modelling

In order to reverse engineer optical data from the photographed brightness a semi-empirical model was developed. Using the setup in figure 4, the light seen by the observer, e.g. the camera, can be written as (Incropera et al., 2007)

$$I_c = \rho_S\ I_i + \rho_D\ \frac{cos\Theta}{\pi}\ G, \tag{2}$$

where I_c, I_i and G denote the intensity, seen by the camera, incident intensity and hemispherical incident intensity, respectively, as shown in figure 4 here. ρ_S and ρ_D are the specular and diffuse reflectance of the radiated area. Eventually Θ depicts the off-axis angle of the camera.

Assuming the camera efficiency to be constant over wavelength, the intensity at the camera and seen brightness, e.g. as pixel values, can be correlated by $I_c = C_{BI}\,B_c$, where C_{BI} is a constant correlation factor. Introducing the

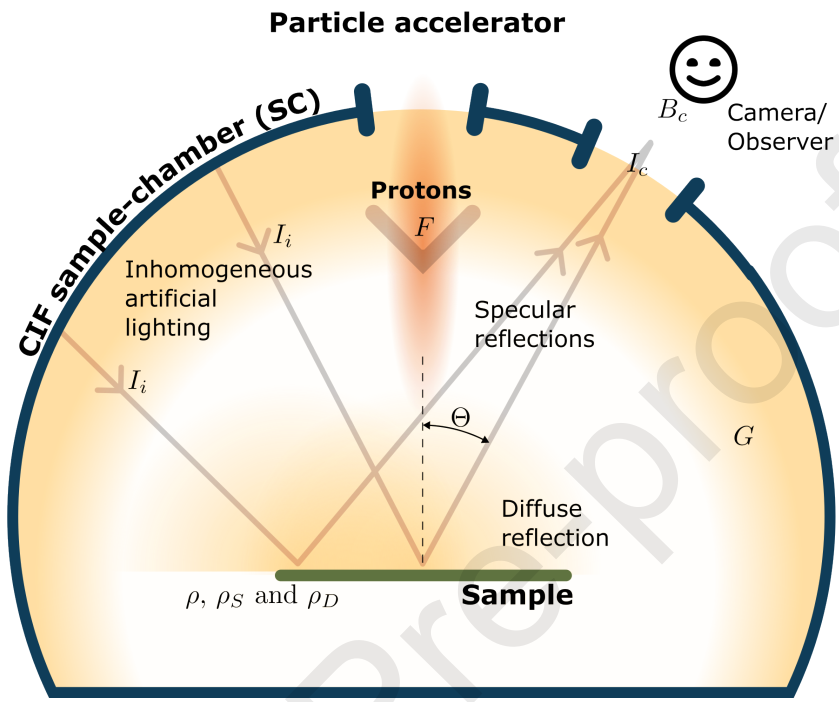

Figure 4: Principal sketch of the CIFs sample chamber. Indicated are direction of proton irradiation as well as direction of observation via camera. Specular and diffuse reflections are also depicted. The inhomogeneous lighting causes a pattern to be seen on the sample which is visible in figure 2. Depiction not to scale.

specular and diffuse reflectance factors, $s = \rho_s/\rho$ and $d = \rho_d/\rho$ respectively, and exchanging I_c with B_c, equation 2 becomes

$$B_c = \rho\left[s\,\frac{I_i}{C_{BI}} + d\,\frac{cos\Theta}{\pi}\,\frac{G}{C_{BI}}\right]. \tag{3}$$

Here s and d are connected by $1 = s + d$ and setting the total reflectance ρ also determines the absorption α, thus the optical properties of interest are fully described.

In order to make an extrapolation of the behaviour, a describing function has to be chosen, that can be inserted into equation 3, fitted to the brightness data shown in figure 3 and eventually extrapolated. Therefore an empirical function from Dachwald et al. (2005) was adapted:

$$p(F) = \begin{cases} p_0 & \text{if } F \leq F_0 \\ p_0 + \Delta p \Big[1 - exp(-(F - F_0)\,\lambda) \Big] & \text{otherwise.} \end{cases} \quad (4)$$

In above equation p denotes an arbitrary thermo-optical property dependent on the orthogonally incident proton fluence F such as the reflectance factor s in equation 3. p_0 is the initial value and $p_\infty = p_0 + \Delta p = \lim_{F\to\infty} p(F)$ the final value. F_0 and λ characterize a fluence offset and half-life proton fluence (Dachwald et al., 2005) respectively. The offset fluence was included as each sample clearly exhibited a different behaviour as to when the brightness started changing, most distinctive for sample S1, see figure 3.

Using equation 4 to describe the specular reflectance factor s and total reflectance ρ, replacing the diffuse reflectance factor d with $(1-s)$ and inserting this into equation 3 gives:

$$B_c(F) = \rho(F) \left[s(F)\,\frac{I_i}{C_{BI}} + (1 - s(F))\,\frac{cos\Theta}{\pi}\,\frac{G}{C_{BI}} \right] \quad (5)$$

In order to be able to fit the independent parameters of $s(F)$ and $\rho(F)$ to the recorded brightness, the constants $\frac{I_i}{C_{BI}}$ and $\frac{G}{C_{BI}}$ have to be determined. Assuming that the illumination was constant throughout the entire process, ex-situ initial and post-irradiation total, specular and diffuse reflectance can be inserted into equation 5, which produces two equations thus that the constants can be solved for.

It should be mentioned, that it is reported, that samples tend to brighten up, e.g. part of the damage due to irradiation is reversed, again when exposing them to atmosphere after irradiation (Sheikh, 2016), which can cause deviation of the constants $\frac{I_i}{C_{BI}}$ and $\frac{G}{C_{BI}}$. Additionally, the authors of this publication experienced the healing of the investigated samples to a certain degree, thus time between irradiation, exposure to atmosphere and spectroscopy does play a role. The reversibility of the blistering effect, that was observed on S4 and S5 happened in the time scale of several years stored at room temperature (RT) under atmosphere. Whether or not this self healing can also occur in vacuum is to be investigated in future studies.

In favour of simplicity it is assumed, that $\rho(F)$ and $s(F)$ share the same F_0 and λ, which leaves 4 total fitting parameters, being $\Delta\rho$, Δs, F_0 and λ. To increase model simplicity, reflectance is also taken to be constant in a separated fitting process, e.g. $\Delta\rho = 0$. Comparisons will be shown in section 3.

3. Results

Fitting the parameters of the function introduced in section 2.3 was restricted to the actual use-case namely the irradiation itself. In figure 5 both, original data and fitted brightness with constant total reflectance, is plotted. Fitted data with variable total reflectance looked very similar which can be seen in table A.2.

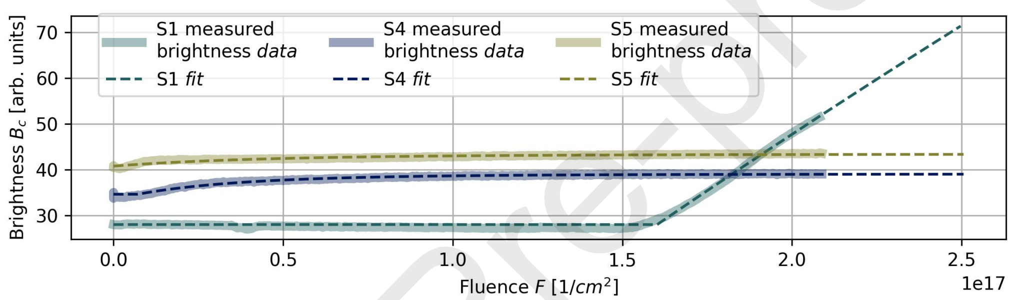

Figure 5: Side by side plot of original data and fitted functions with constant total reflectance. Fitted data is extrapolated beyond irradiation. Original data only plotted for irradiation.

Eventually the specular reflectance, including error propagation, is plotted in figure 6. Error analysis includes standard deviation of initial measurements of specular and total reflectance, as written in table 1, and the fitting error given by the least-square fit. Shown is the fit with constant total reflectance. As can be seen in table A.2, the deviation of the specular reflections with variable total reflectance is higher.

The R^2 values given in table A.2 indicate good agreement with the original data.

Eventually figure 7 shows the fitting parameter, describing the thermo-optical properties' behaviour, over temperature. Additionally a trend line derived from linear regression is plotted. The polynomial parameters for the first-order fit are shown in table A.3. They will be discussed later in section 5.

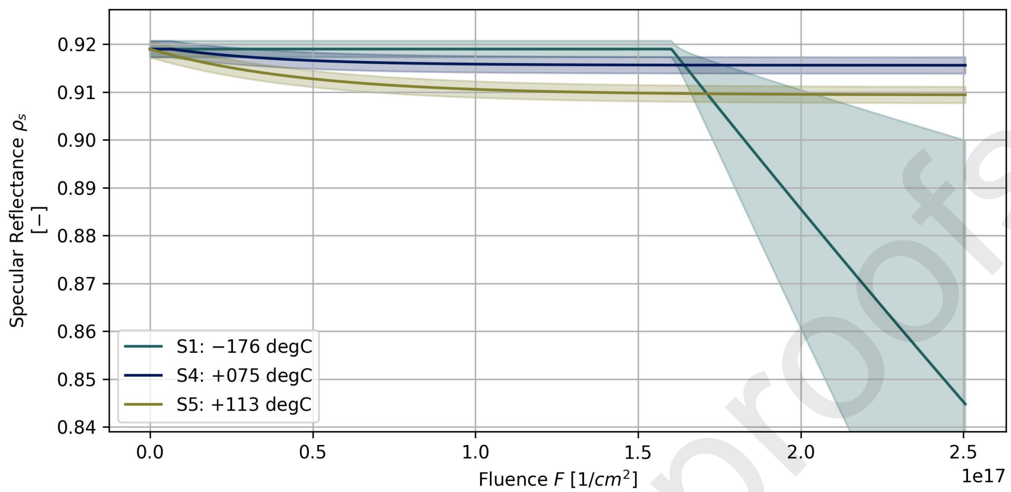

Figure 6: Plot of the specular reflectance over fluence including uncertainty propagation.

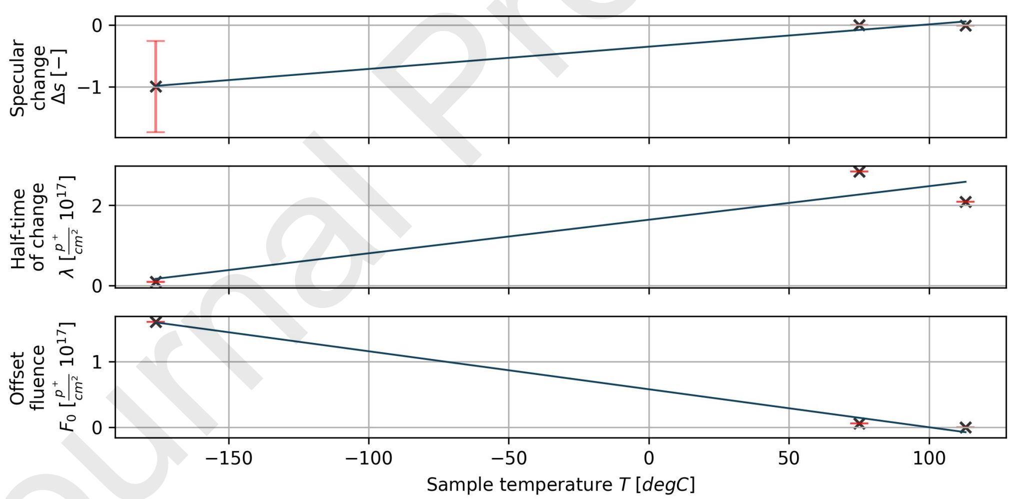

Figure 7: Fitting parameter of the specular reflectance (with constant total reflectance). Also given is a trend line derived by linear regression. Parameters of the fit can be seen in table A.3. The red error bars denote the fitting uncertainty.

From figure 7 it becomes clear, that for increasing temperature, the specular reflectivity reduction decreases. Furthermore, the hotter the surface, the slower the process of blistering progresses, seen in the regression of the half-time λ. Eventually, the colder the temperature, the later the process starts to take effect, depicted by the offset fluence F_0. These trend lines have to be taken with care, as the available data does not allow to give a final statement on the actual behaviour.

Concluding this section, the developed model is depicted in figure 8. Initially the mission trajectory defines proton flux and temperature of the membrane. Flux and mission duration define the fluence at e.g. End Of Life (EOL). Given the temperature the fitting parameters can be interpolated as shown in figure 7.

Here a linear regression has been used due to lack of data points. Parameters p_i^X can be found in table A.3. X denotes the variable in question, see figure 8 for further explanation. With added empirical data a polynomial fit of order two and higher can become more accurate, but is not scope of this publication. Eventually the fitting parameters can be inserted into equation 4. For constant total reflectance, s is to be multiplied with the initial ρ in order to get the specular reflectance.

The mechanical degradation has not been part of the investigated material parameter set. Degradation of the substrate material of the membrane is not expected since the penetration depth of the used radiation does not or only a fraction reach its depth, see figure A.10.

4. Discussion

As seen in the previous sections, it is possible to derive reflectance values from time-lapse images taken during irradiation.

In the previous publication (Sznajder et al., 2020) it was stated that total reflectance is changing for irradiation at low temperatures. The new results argue, that the total reflectance change is partially caused by annealing after irradiation of the cold samples S1 and S2. For the warmer samples, S3 to S5, total reflectance can be assumed to be constant, which indicates, for the fluence and temperatures investigated in this study, the total reflectance can be taken as constant throughout the solar sail mission.

From figure 7 the dependence on temperature of the fitting parameter can be seen. The higher the temperature, the sooner, faster and smaller the change is. Although the trending lines are indicating this, the offset fluence cannot be smaller than zero. Likewise, it is not to be expected that Δs will be higher than zero, meaning that the blistering is unlikely to cause an

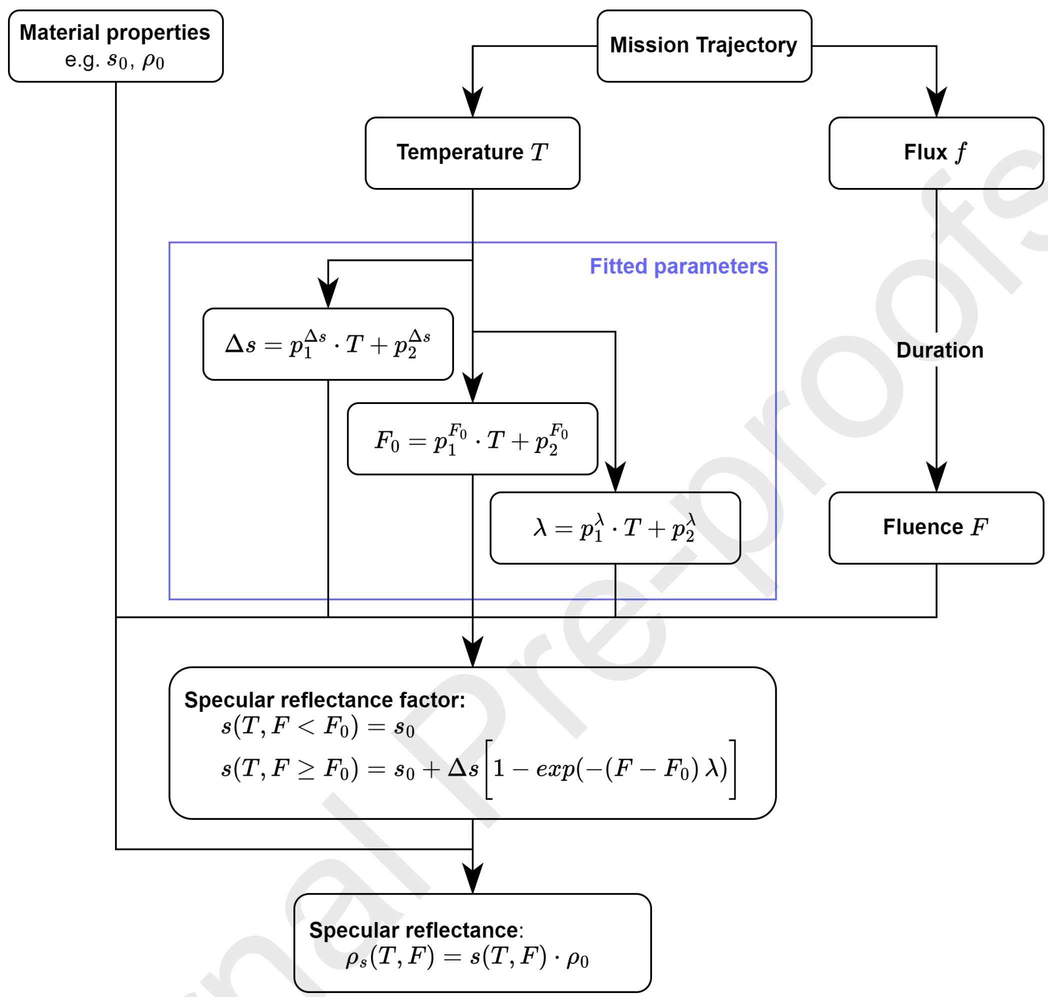

Figure 8: Flowchart of the semi-empirical model with constant total reflectance. Initially, from the mission trajectory follows flux and temperature of the solar sail. Duration defines fluence and temperature sets the parameters for determination of the specular reflectance factor. Eventually specular reflectance is calculated by including the total reflectance.

increase in specular reflectance at constant temperature and flux. Similarly the specular reflectance factor change Δs cannot be below $1 - s_0$, depending on the initial specular reflectance factor s_0, since s itself can only assume values between 0 and 1.

For sample S1, the specular reflectance factor, where $F \to \infty$, goes towards 0. E.g. $s_\infty = s_0 + \Delta s = 0.9957 - 0.9957$ for constant total reflectance (see table A.2), suggesting, that at some point, aluminized membranes at -173 °C will only reflect diffusely. This requires the membrane to be constantly at -173 °C, a minimum flux (Sznajder et al., 2018) in order to counter removal of H^+ by diffusion and a minimum fluence for the blistering phenomena to occur (Sznajder et al., 2015).

Figure 9 shows the complex interplay of the modelling parameters indicating that the specular reflectance change at temperature of approximately -50 to -100 °C is higher than for lower temperature after irradiation of $2.5 \cdot 10^{17} p^+/cm^2$. This is confirmed by samples S2 (-100 °C, $\rho_S = 0.479$), see table 1, for which unfortunately no time-lapse data was available, but fits qualitatively well into the developed model. S3 (31.6 °C, $\rho_S = 0.781$) matches also well the data. Unfortunately reflectance measurements can not be directly compared with the model output, because e.g. samples S1 and S2 had to be heated to RT in order to remove them from the vacuum, which influenced the reflectance of the surfaces, which can be seen exemplary in figure 3 for S1.

Assuming that the AF of the laboratory irradiation has no influence on the blistering process and hence changing flux in orbit has no effect, figure 9 is valid for any arbitrary mission trajectory where the sail temperature is kept constant. As seen for sample S1, changing temperature can have drastic influence on the opritcal properties.

The typical solar sail mission trajectory experiences temperature gradients (Sznajder et al., 2020). Increasing or decreasing temperature can cause altered behaviour of the specular reflectance change. Behaviour of S1 in figure 3 after irradiation and during heating can give an idea for this. Depending on the accumulated hydrogen inside the top layers of the sail membrane, increasing temperature can drastically worsen the specular reflectance, since the increased diffusion enables the hydrogen to form H_2-blisters. Contrary, the membrane having a higher temperature from the start of exposure to proton radiation prevents the accumulation and hence blister formation. This being said, the solar sail mission trajectory should be designed such that either this scenarion of cold hydrogen agglomeration and following heating is avoided or by either heating or manipulating the thermo-optical properties. Including heating infrastructure could add unnessecary weight to the system such that a trade-off with possible degradation could still be a working solution.

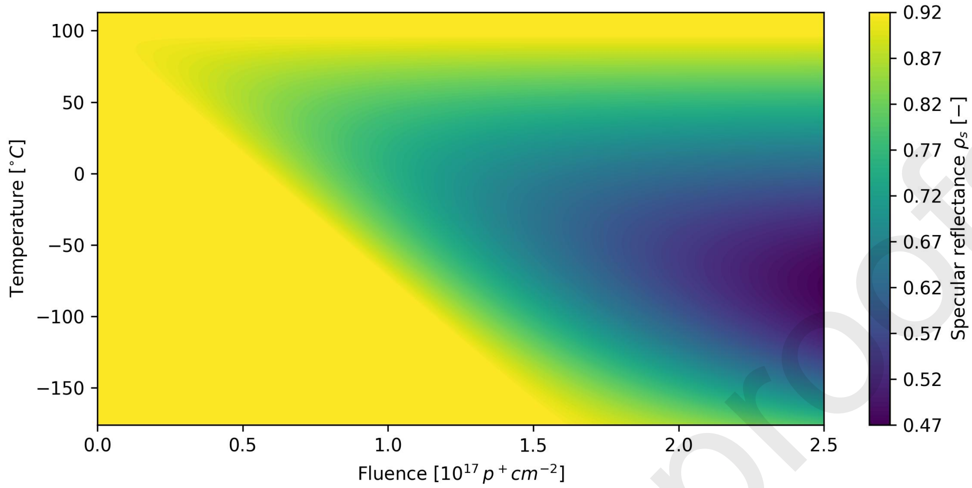

Figure 9: Specular reflectance over fluence and temperature using the procedure in figure 8..

5. Conclusion

A semi-empirical model has been developed, that, with given mission flux and temperature, can estimate the development of the specular or diffuse reflectance. The outcome is shown in figure 9. In figure 8 the work flow has been shown that results in the specular reflectance over fluence and temperature.

With concerns to the performance of solar sail membranes, hotter temperatures seem to be optimal for solar sailing with aluminized layers as here the diffuse reflectance is reduced to a minimum. On the other side, the mission duration has to be taken into account. Cold temperature, below -100 °C, delay effects of the agglomerating hydrogen onto the surface, hence any reflectance change could occur after EOL, where it has no influence on the sail performance during mission but could possibly harm the sails performance when heated since agglomerated hydrogen than could get enough movability to quickly form blisters. Hence, for any mission trajectory the thermal management has a big influence on the thermo-optical properties and hence performance of the sail itself.

The characteristic acceleration remains nearly unchanged when the total reflectance is constant, showing that variations in specular reflectance have only a minor influence on this parameter. E.g. a sail that reflects purely diffusely has a characteristic acceleration of 89.95 % (Sznajder et al., 2020) compared to an unaltered sail membrane. Consequently, it is of subordinate importance to calculate the characteristic acceleration from specular reflectance data obtained using a model that assumes constant total reflectance, since even small deviations in total reflectance would have only a negligible effect on the resulting acceleration. However, the total reflectance is a key parameter for the performance of solar sail and hence an extensive model incorporating the prediction of total reflectance is required but outside of the scope of the here presented data.

Concluding, the here introduced semi-empirical model is able to derive total, specular and diffuse reflectance from recorded time-lapse images during irradiation with thermo-optical properties measured before and after irradiation test. The information can be used to approximate the reflectance degradation over mission fluence given the fitting parameters in table A.2 and as shown in figure 8. Thus, e.g., the acceleration of a solar sail can be calculated over mission time considering potential degradation due to proton irradiation. At the moment this is for constant temperature and flux.

6. Outlook

The data on which this semi-empirical model is based is rather restricted. Hence, for ongoing refinement of the model, further experiments are needed with various proton energies and temperatures, including temperature gradients found on a solar sail mission, can be investigated.

The sudden increase in H diffusion with agglomerated protons, and hence hydrogen, in the lattice can cause major reflectance changes to onset rapidly when the temperature of the sail membrane increases. This sparks interest in the time-temperature dependency on diffusion rates and consequently whether longer term irradiations at lower fluxes will induce the same damage due to natural diffusion of protons out of the metal lattice.

In addition to extra variables and expanded dataset capture, the optical set-up can also be refined to reduce the stray light contributions of G and I_i, through use of light absorbing baffles and optical masking.

Another key aspect of interest in future experimental campaigns is the effect of a combined proton, electron and Ultra Violet (UV) light irradiation to better replicate the space environment and to test if emergent effects arise from the interplay of all three sources.

7. Acknowledgements

This work was conducted at the German Aerospace Center (DLR) research and development branch, and partially supported (M. Sznajder) by a program of the Polish Ministry of Science under the title *Regional Excellence Initiative*, project no. RID/SP/0050/2024/1.

8. Data Availability Statement

The original contributions presented in the study are included in the article/appendix, further inquiries can be directed to the corresponding author.

364 ## Appendix A. Supplementary Data

365 *Likelihood of implantation into Upilex membrane*

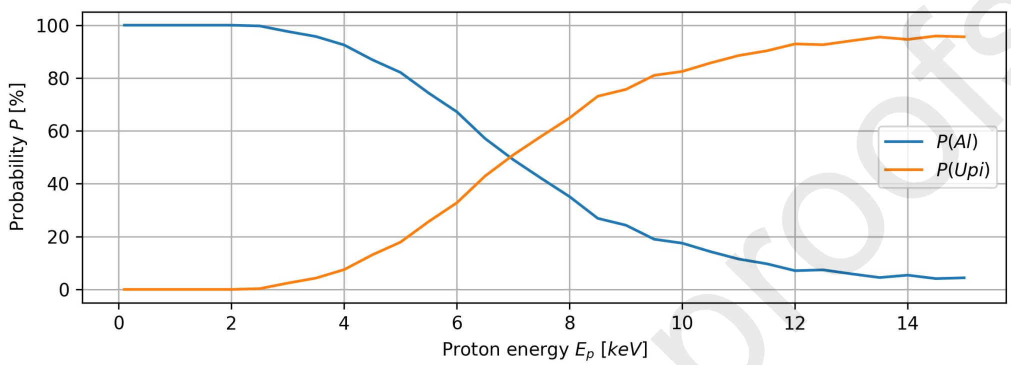

Figure A.10: Probabilities of protons with given energy implanting into layers of aluminized Upilex membrane. $P(Al)$ and $P(Upi)$ denote implantation into aluminium and Upilex layer respectively. Aluminium layer is 100 nm thick, Upilex anything below. Any aluminium oxide at surface has been neglected for this calculation.

Fitting parameters for semi-empirical model

Table A.2: Fitting parameter including uncertainties and further determining variables of the modelling environment. Graphs are shown in figure 5. Grey background indicates changing total reflectance, for white the total reflectance was not allowed to change during irradiation.

Sample	Δs	$\Delta \rho$	λ	F_0	R^2
S1	-0.9957 ± 0.7358	-	$9.3 \cdot 10^{-2}$ $\pm 6.7 \cdot 10^{-3}$	1.6024 $\pm 4.3 \cdot 10^{-6}$	0.993
S1	-0.9957 $\pm 5.7 \cdot 10^{4}$	$-4.9 \cdot 10^{-23}$ $\pm 1.2 \cdot 10^{4}$	$9.3 \cdot 10^{-2}$ $\pm 4.7 \cdot 10^{2}$	1.6024 $\pm 7.7 \cdot 10^{-6}$	0.993
S4	$-3.7 \cdot 10^{-3}$ $\pm 7.3 \cdot 10^{-11}$	-	2.8363 $\pm 1.3 \cdot 10^{-3}$	$6.5 \cdot 10^{-2}$ $\pm 5.6 \cdot 10^{-6}$	0.979
S4	$-1.0 \cdot 10^{-2}$ $\pm 2.2 \cdot 10^{-5}$	-0.1529 $\pm 8.2 \cdot 10^{-3}$	2.1085 ± 0.5713	$7.2 \cdot 10^{-2}$ $\pm 5.4 \cdot 10^{-6}$	0.982
S5	$-1.0 \cdot 10^{-2}$ $\pm 4.2 \cdot 10^{-9}$	-	2.0873 $\pm 3.3 \cdot 10^{-3}$	$1.4 \cdot 10^{-17}$ $\pm 3.7 \cdot 10^{-5}$	0.868
S5	$-3.5 \cdot 10^{-2}$ $\pm 2.6 \cdot 10^{-3}$	-0.1128 $\pm 4.1 \cdot 10^{-2}$	1.5698 ± 2.4552	$5.5 \cdot 10^{-11}$ $\pm 3.4 \cdot 10^{-5}$	0.880

Table A.3: Linear regression parameter describing temperature dependence of fitting parameter shown in table A.2. Usage is shown in figure 8 and 9.

Parameter	p_1	p_2
Δs	0.00360538	-0.35100396
F_0	-0.00575478	0.57874905
λ	0.00835543	1.63884696

References

Agency, E.S., 1993. Radiation Design Handbook. Technical Report. European Space Agency.

Dachwald, B., 2010. Solar Sail Dynamics and Control, in: Blockley, R., Shyy, W. (Eds.), Encyclopedia of Aerospace Engineering. Wiley, Chichester. doi:10.1002/9780470686652.eae292.

Dachwald, B., Seboldt, W., Macdonald, M., Mengali, G., Quarta, A., McInnes, C., Rios-Reyes, L., Scheeres, D., Wie, B., Görlich, M., Lura, F., Diedrich, B., Baturkin, V., Coverstone, V., Leipold, M., Garbe, G., 2005. Potential Solar Sail Degradation Effects on Trajectory and Attitude Control, in: Guidance, Navigation, and Control and Co-located Conferences: AIAA Guidance, Navigation, and Control Conference and Exhibit, American Institute of Aeronautics and Astronautics, San Francisco. doi:10.2514/6.2005-6172.

Daniels, R.D., 1971. Correlation of Hydrogen Evolution with Surface Blistering in Proton-Irradiated Aluminum. Journal of Applied Physics 42, 417–419. doi:10.1063/1.1659613.

Eichler, J., 2005. Lectures on Ion-Atom Collisions: From Nonrelativistic to Relativistic Velocities. Elsevier.

Hagstrum, H.D., 1954. Theory of Auger Ejection of Electrons from Metals by Ions. Physical Review 96, 336–365. doi:10.1103/PhysRev.96.336.

Incropera, F.P., DeWitt, D.P., Bergman, T.L., Lavine, A.S. (Eds.), 2007. Fundamentals of Heat and Mass Transfer. 6. ed. ed., Wiley, Hoboken, NJ.

Klein, E.M., Sznajder, M., Seefeldt, P., 2022. Proton Spectra for the Interplanetary Space Derived From Different Environmental Models. Frontiers in Space Technologies 3, 14. doi:10.3389/frspt.2022.933340.

Milacek, L.H., Daniels, R.D., Cooley, J.A., 1968. Proton-Radiation-Induced Blistering of Aluminum. Journal of Applied Physics 39, 2803–2815. doi:10.1063/1.1656677.

Myers, S.M., Baskes, M.I., Birnbaum, H.K., Corbett, J.W., DeLeo, G.G., Estreicher, S.K., Haller, E.E., Jena, P., Johnson, N.M., Kirchheim, R., Pearton, S.J., Stavola, M.J., 1992. Hydrogen interactions with defects in crystalline solids. Reviews of Modern Physics 64, 559–617. doi:10.1103/RevModPhys.64.559.

Renger, T., Sznajder, M., Witzke, A., Geppert, U.R., 2014. The complex irradiation facility at DLR-Bremen, in: Advances in Solar Sailing. Springer, pp. 541–557.

Sheikh, D.A., 2016. Improved silver mirror coating for ground and space-based astronomy, in: Advances in Optical and Mechanical Technologies for Telescopes and Instrumentation II, SPIE. pp. 1007–1013. doi:10.1117/12.2234380.

Sols, F., Flores, F., 1984. Charge transfer processes for light ions moving in metals. Physical Review B 30, 4878–4880. doi:10.1103/PhysRevB.30.4878.

Sznajder, M., 2023. Solar wind H+ fluxes at 1 AU for solar cycles 23 and 24. Advances in Space Research 71, 4923–4957. doi:10.1016/j.asr.2023.01.054.

Sznajder, M., Geppert, U., Dudek, M., 2015. Degradation of metallic surfaces under space conditions, with particular emphasis on Hydrogen recombination processes. Advances in Space Research 56, 71–84. doi:10.1016/j.asr.2015.03.032.

Sznajder, M., Geppert, U., Dudek, M.R., 2018. Hydrogen blistering under extreme radiation conditions. npj Materials Degradation 2, 1–8. doi:10.1038/s41529-017-0024-z.

Sznajder, M., Seefeldt, P., Spröwitz, T., Renger, T., Kang, J.H., Bryant, R., Wilkie, W., 2020. Solar sail propulsion limitations due to hydrogen blistering. Advances in Space Research 67, 2655–2668. doi:10.1016/j.asr.2020.06.034.

Ziegler, J.F., Ziegler, M.D., Biersack, J.P., 2010. SRIM – The stopping and range of ions in matter (2010). Nuclear Instruments and Methods in Physics Research Section B: Beam Interactions with Materials and Atoms 268, 1818–1823. doi:10.1016/j.nimb.2010.02.091.

Declaration of Interest Statement

☒ The authors declare that they have no known competing financial interests or personal relationships that could have appeared to influence the work reported in this paper.

☐ The author is an Editorial Board Member/Editor-in-Chief/Associate Editor/Guest Editor for this journal and was not involved in the editorial review or the decision to publish this article.

☐ The authors declare the following financial interests/personal relationships which may be considered as potential competing interests: